The International Journal of Advanced Manufacturing Technology (2022) 119:3903–3916
https://doi.org/10.1007/s00170-022-08650-1

ORIGINAL ARTICLE

Development and verification of six-degree-of-freedom error measurement system based on geometrical optics for linear stage

Wei-Che Tai[1] · **Chien-Sheng Liu**[1]

Received: 28 September 2021 / Accepted: 30 December 2021 / Published online: 10 January 2022

Abstract
In this paper, a six-degree-of-freedom (6DOF) error measurement system based on geometric optics is proposed for linear stages. This measurement system uses an additional linear stage that drags the sensor onto the stage so that the light spot projected on the sensor moves back and forth with the moving stage. This method achieves long-range 6DOF measurement. Compared with commercial laser interferometers, the proposed measurement system has the advantages of a lower cost, a simpler structure, and the capability of measuring 6DOF errors simultaneously. Zemax software was used to simulate the relationships between the 6DOF errors and the values of position-sensitive detectors. MATLAB software was then used to construct the forward and inverse mathematical kinematic models of the optical paths and simplify the models through curve fitting. Finally, to address installation and manufacturing errors, a reverse kinematic mathematical solution was obtained through the use of a six-axis Stewart platform. The proposed measurement system was experimentally implemented on a commercial linear stage to measure the 6DOF errors and verified against results obtained with a commercial interferometer and electronic level.

Keywords Geometric errors · Skew-ray tracing · Six-degrees-of-freedom error measurement · Linear stage of machine tool · Error decouple · Crosstalk

1 Introduction

The demand for precision measurements is increasing rapidly with advances in science and technology. As machining processes become more sophisticated, more efficient multiaxis machine tools with greater accuracy are required [1, 2]. The linear stage is a key and indispensable component of multiaxis machine tools, regardless of their function or configuration. Because the linear stage is used primarily to move the workpiece or tool according to the machine configuration, its accuracy directly affects the final product [3–7].

As a result of deviations in the manufacturing and assembly of the components of linear stages, positioning (δ_y) and five other geometric errors (horizontal straightness δ_x, vertical straightness δ_z, pitch ε_x, roll ε_y, and yaw ε_z) are created [8–12]. Geometric errors are crucial causes of inaccurate positioning in multiaxis machining, and numerous studies have investigated the measurement of and compensation for such geometric errors [13]. Among these geometric errors, positioning error has a large influence on the precision and defect-free rate of manufacturing. To improve the accuracy of multiaxis machine tools, a method of measuring six-degree-of-freedom (6DOF) geometric errors is necessary.

Interferometry is an accurate method of noncontact measurement for multiaxis machine tools, and laser interferometry has been widely used to measure the geometric errors of linear stages because of its high resolution and long-range measurement capacity. However, laser interferometry can be used to measure only a single geometric error at a time, limiting its measurement efficiency and accuracy. This complex procedure requires individual procedures and optical accessories to resolve each geometric error and may require several hours, or even days, to measure the geometric errors of a multiaxis machine tool. Measurement interrupts the production process [14] and is thus costly [15, 16]. In addition, the crosstalk among error components creates additional complexity [17] because it can considerably influence measurement accuracy [18–20].

✉ Chien-Sheng Liu
csliu@mail.ncku.edu.tw

[1] Department of Mechanical Engineering, National Cheng Kung University, No. 1, University Road, Tainan City 70101, Taiwan

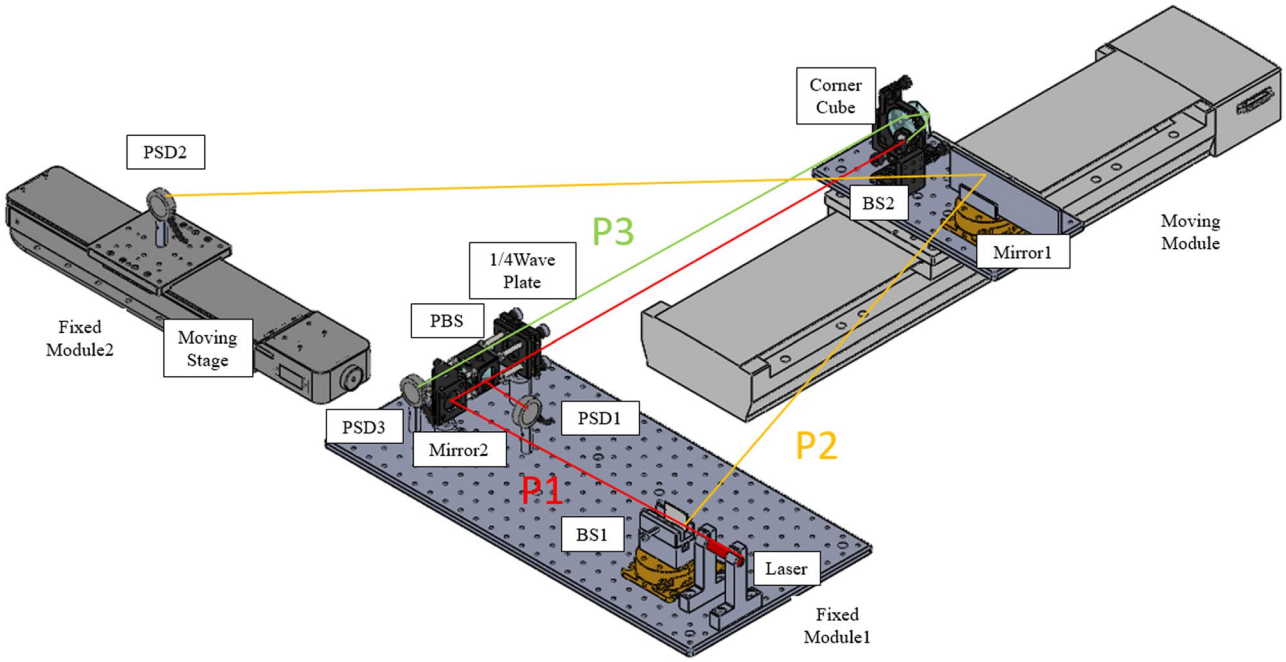

Fig. 1 Proposed measurement system

To enhance the efficiency and accuracy of measurement, multi-DOF (MDOF) errors must be clarified simultaneously. Various methods for measuring MDOF geometric errors have been proposed. Based on different metrologies, such measurement systems can be classified into those utilizing only interferometry [21, 22] or those utilizing geometrical optics combined with interferometry [23–29]. Furutani et al. presented a 6DOF geometric error measurement system using a Michelson interferometer for linear stages [21]. However, if all errors are measured through interferometry, calculation becomes more complex. Therefore, scholars such as Feng et al. have proposed measuring 6DOF geometric error through simultaneous interferometry and geometric optics [26].

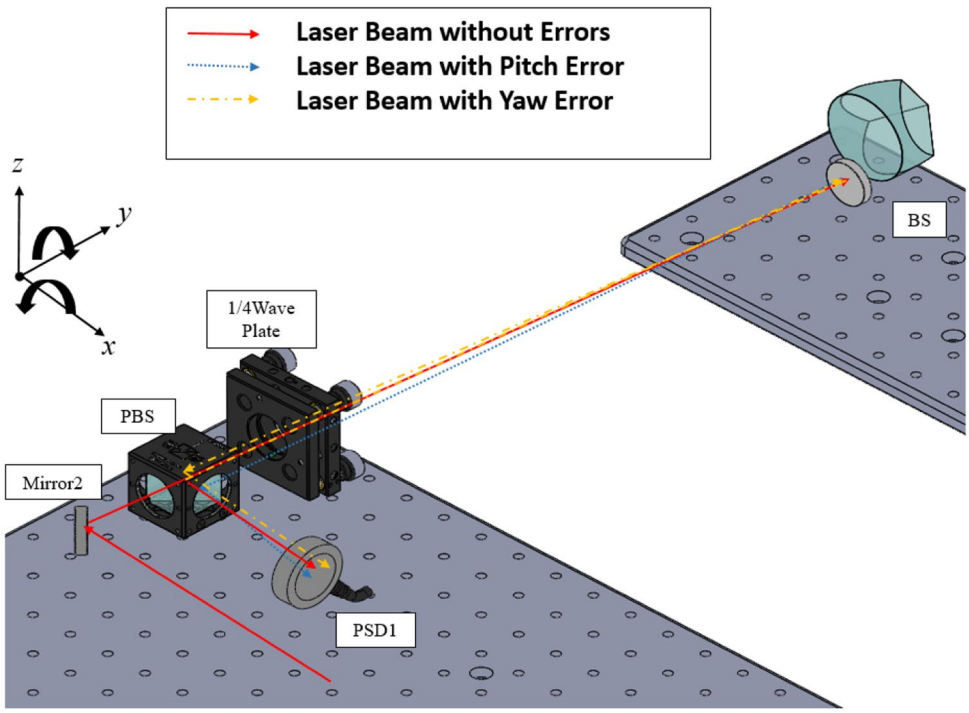

Fig. 2 Light path P1 with pitch or yaw error

Although the geometric optic measurement method has measurement range and resolution limitations, it can provide simpler and cheaper measurements. Therefore, an increasing number of scholars are focusing on this method. For example, Zheng et al. proposed a system for measuring 21 geometric motion errors for three linear stages [27], and Huang et al. proposed an embedded sensor system for measuring five-DOF geometric errors [28]. Liu et al. presented a system for measuring 6DOF errors for translation stages; the system involves adjusting the direction of the laser beam to ensure that the spot is always on the sensing area of the position-sensitive detector (PSD) of a long linear stage [29]. However, the accuracy of measurement systems based on geometrical optics can be influenced by systematic errors, such as those relating to the installation and manufacturing of the stage components [29, 30]. Accordingly, to improve measurement accuracy, we developed a long-range 6DOF error measurement system based on geometrical optics and method of compensating for systematic errors.

2 System configuration

The proposed measurement system consists of a moving module and two fixed modules, as presented in Fig. 1. Fixed modules 1 and 2 are installed outside the linear stage, and the moving module is installed on the stage. Fixed module 1 comprises a red laser source (632 nm), beam splitter (BS1), polarizing beam splitter (PBS), mirror, quarter-wave plate, and two PSDs (PSD1 and PSD3). Fixed module 2 consists

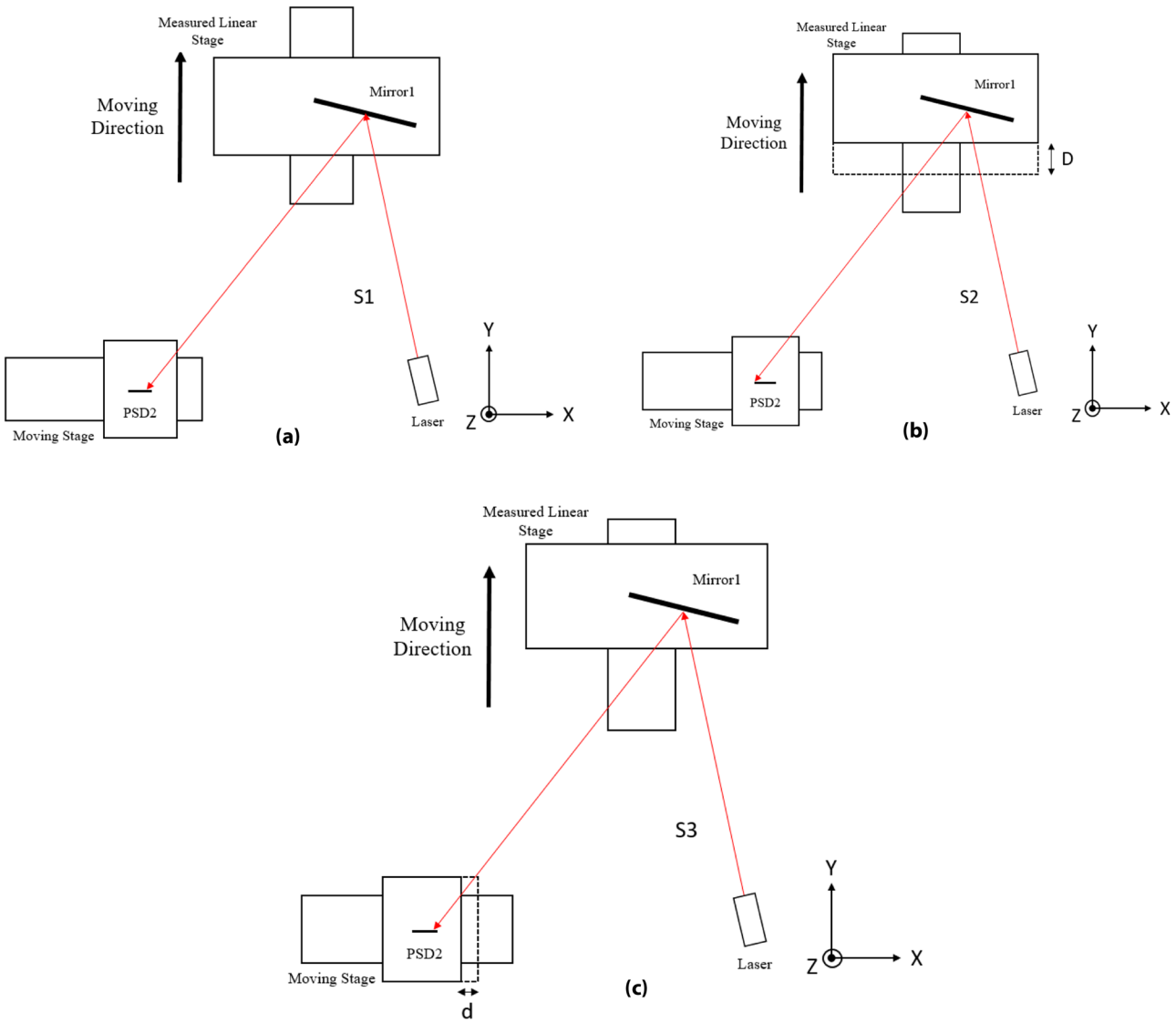

Fig. 3 Measurement principle of long-range positioning error

of a PSD (PSD2) and an additional linear stage that can drag PSD2 to track the light spot so that the laser is always projected onto PSD2. The moving module includes a beam splitter (BS2), corner cube, and mirror (mirror1). When the measured linear stage moves, the laser beam is adjusted on the basis of the 6DOF geometric errors and geometric optics, and the function of the moving module is to reflect the beam adjusted by the 6DOF geometric errors onto the PSDs.

3 Measurement principle

The proposed measurement system includes three light paths, P1 (Fig. 2), P2, and P3. The laser transmits the PBS because it is P polarized, and the transmitted beam then passes through the BS2 on the moving module after the quarter-wave plate and becomes S polarized light, which is subsequently reflected from the PBS to PSD1. The system is sensitive only to pitch and yaw errors because of the layout of the geometrical optics.

The light path P2 is the key to the long-range measurement of positioning error (Fig. 3). P2 uses a simple triangulation method based on geometric optics [31]. The laser is first reflected by mirror1 and received by PSD2, which is installed on the additional linear stage, which uses PSD2 to track the laser spot.

As illustrated in Fig. 3a and b, when the measured linear stage moves forward a distance D, the light path changes from the light subpath S1 to S2, causing the laser spot to move from the start to the end position; PSD2 then captures the position data of each start and end point to calculate the positioning error through subtraction. In S2, the laser beam is near the left-hand limit of PSD2; therefore, the additional linear stage (under PSD2) is moved by a displacement d, moving the relative position of the laser spot to the right-hand limit of PSD2 (Fig. 3c), which is then ready for the next displacement. Thus, when the additional linear stage moves forward d, the PSD2 sensing area is extended to achieve long-range measurement. However, the additional linear stage featuring PSD2 also possesses 6DOF geometric errors, which are discussed in Sect. 5.

In the light path P3 (Fig. 4), the laser beam passes through the BS and the corner cube. Because of the corner cube's unique structure, it can double the ability of the system to detect the horizontal and vertical straightness errors.

4 Optical simulation and mathematical modeling

4.1 Optical simulation

Numerical simulations in Zemax optical simulation software were used to confirm the feasibility of the proposed measurement system (Fig. 5). Figure 6 provides the PSD value changes resulting from the positioning, horizontal

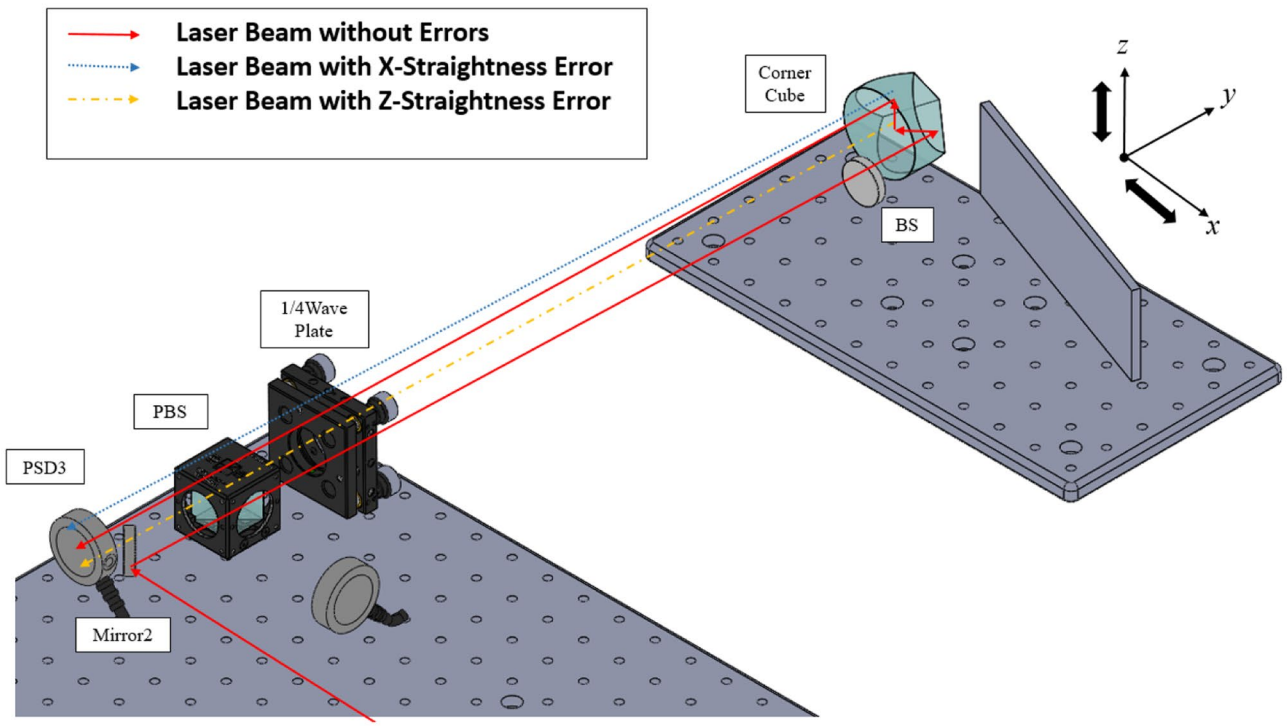

Fig. 4 Light path P3 with horizontal straightness error or vertical straightness error

straightness, vertical straightness, pitch, yaw, and roll error, demonstrating that every type of error could be captured by the PSDs; thus, all the errors can be calculated using further proposed mathematical models. In the optical simulation, the moving module employs its center as the center of rotation; thus, the 6DOF geometric errors occur at this point.

4.2 Derivation of the mathematical model

A mathematical model of the proposed measurement system was constructed using a homogenous transformation matrix (HTM) and a skew-ray tracing method to calculate the data of the three PSDs [32]. The HTM is used to define the boundaries of each optical component relative to the frame of reference to determine the relationships between the 6DOF geometric errors and the position of the light spot on the PSDs. Using flat boundary surface algorithms in the skew-ray tracing method, we constructed the transformation matrix ${}^{R}\boldsymbol{A}_i$, which represents the transfer matrix of the coordinate system of each optical component i from the reference coordinate system $\boldsymbol{R}$:

$$ {}^{R}A_i = \begin{bmatrix} I_{ix} & J_{ix} & K_{ix} & t_{ix} \\ I_{iy} & J_{iy} & K_{iy} & t_{iy} \\ I_{iz} & J_{iz} & K_{iz} & t_{iz} \\ 0 & 0 & 0 & 1 \end{bmatrix} \tag{1} $$

The incident points on the boundary of the optical component must be calculated sequentially (Fig. 7). For every light path, the laser beam must first be defined as a vector after transmission to next optical component (Table 1), and the direction of the beam changes according to the geometrical optics. The new direction and incident point are then used to determine the following incident point P_i and direction l_i:

$$ {}^{g}\overline{R}_i = \left[{}^{g}\overline{P}_i \ {}^{g}\overline{\mathrm{l}}_i \right]^T = \left[P_{ix} \ P_{iy} \ P_{iz} \ \mathrm{l}_{ix} \ \mathrm{l}_{iy} \ \mathrm{l}_{iz} \right]^T \tag{2} $$

This method is used to generate the coordinate information for all the optical components in Fig. 1 and a mathematical model of each optical path, including for both the linear stage to be measured and the additional linear stage. Therefore, the displacements D and d are also calculated in the proposed mathematical model.

Overall, the 6DOF geometric errors created by the measured linear stage change the light paths slightly, and the PSDs detect such changes. Such changes can be input to the proposed mathematical model, the results of which are presented as six linear and independent equations:

$$ X_{PSD1} = F_{X1}\left(\delta_x, \delta_y, \delta_z, \varepsilon_x, \varepsilon_y, \varepsilon_z\right), \tag{3} $$

$$ Y_{PSD1} = F_{Y1}\left(\delta_x, \delta_y, \delta_z, \varepsilon_x, \varepsilon_y, \varepsilon_z\right), \tag{4} $$

$$ X_{PSD2} = F_{X2}\left(\delta_x, \delta_y, \delta_z, \varepsilon_x, \varepsilon_y, \varepsilon_z\right), \tag{5} $$

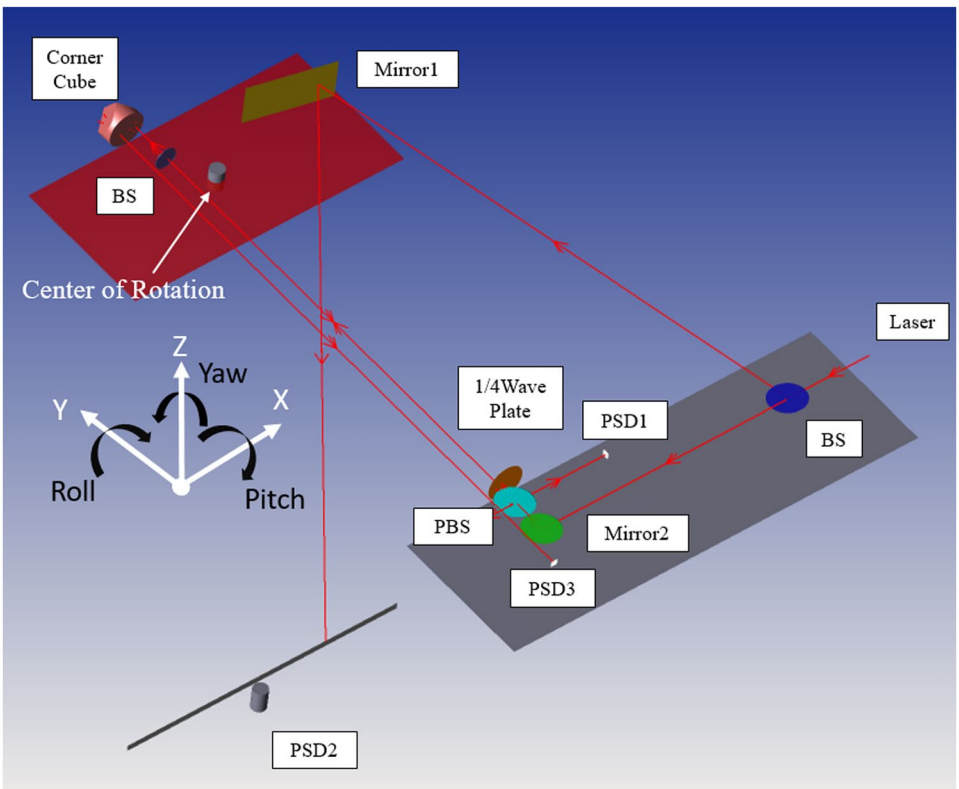

Fig. 5 Optical model of the proposed measurement system

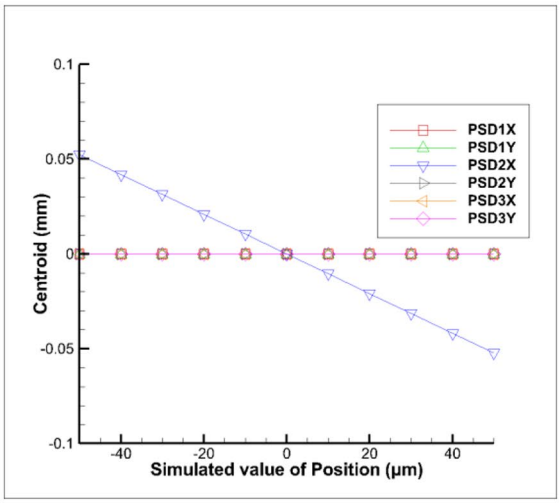
PSD1X
PSD1Y
PSD2X
PSD2Y
PSD3X
PSD3Y
Centroid (mm)
Simulated value of Position (μm)

(a)

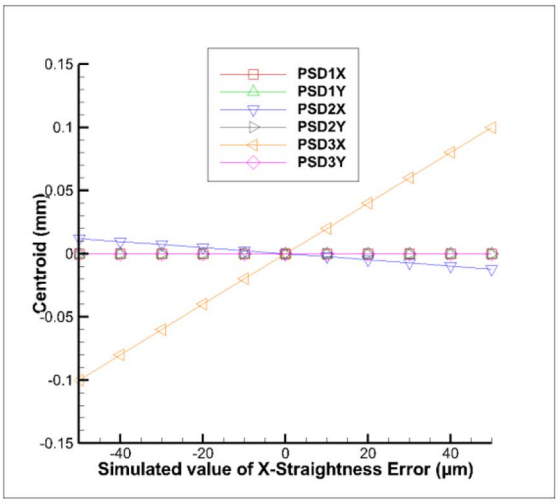
PSD1X
PSD1Y
PSD2X
PSD2Y
PSD3X
PSD3Y
Centroid (mm)
Simulated value of X-Straightness Error (μm)

(b)

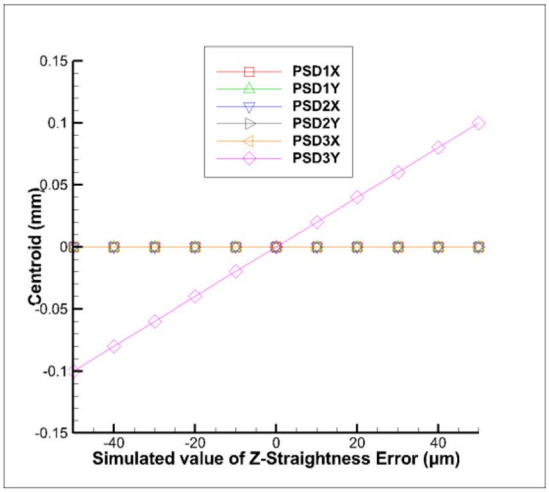
PSD1X
PSD1Y
PSD2X
PSD2Y
PSD3X
PSD3Y
Centroid (mm)
Simulated value of Z-Straightness Error (μm)

(c)

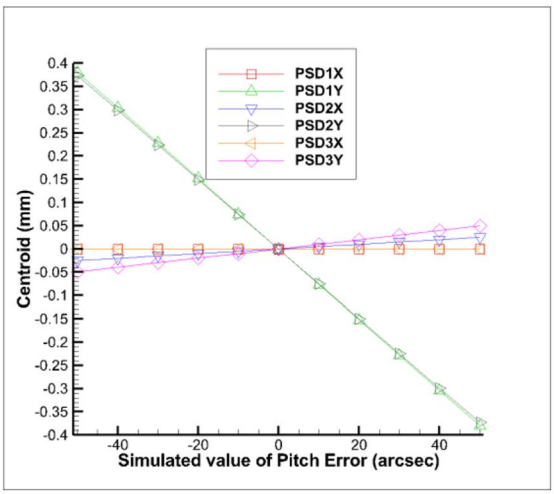
PSD1X
PSD1Y
PSD2X
PSD2Y
PSD3X
PSD3Y
Centroid (mm)
Simulated value of Pitch Error (arcsec)

(d)


PSD1X
PSD1Y
PSD2X
PSD2Y
PSD3X
PSD3Y
Centroid (mm)
Simulated value of Yaw Error (arcsec)

(e)

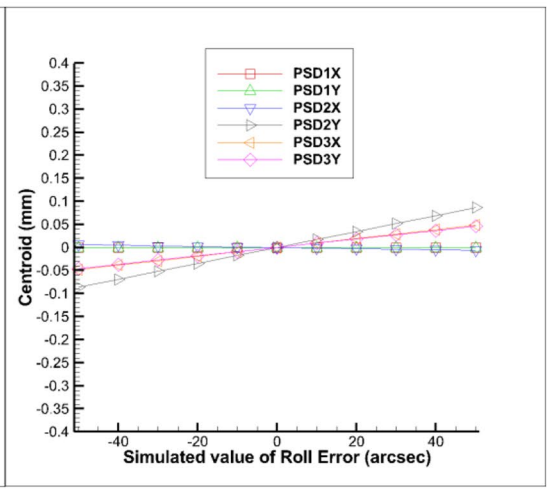
PSD1X
PSD1Y
PSD2X
PSD2Y
PSD3X
PSD3Y
Centroid (mm)
Simulated value of Roll Error (arcsec)

(f)

◂**Fig. 6** Variation of the reading of three PSDs with (**a**) positioning, (**b**) horizontal straightness, (**c**) vertical straightness, (**d**) pitch, (**e**) yaw, and (**f**) roll errors, respectively

$$Y_{PSD2} = F_{Y2}\left(\delta_x, \delta_y, \delta_z, \varepsilon_x, \varepsilon_y, \varepsilon_z\right), \tag{6}$$

$$X_{PSD3} = F_{X3}\left(\delta_x, \delta_y, \delta_z, \varepsilon_x, \varepsilon_y, \varepsilon_z\right), \tag{7}$$

$$Y_{PSD3} = F_{Y3}\left(\delta_x, \delta_y, \delta_z, \varepsilon_x, \varepsilon_y, \varepsilon_z\right). \tag{8}$$

After simplification, Eqs. (3)–(8) can be rewritten as

$$\mathrm{Error}_{N\times 6} = \mathrm{PSD}_{N\times 6} \times \left[\left(\beta_{6\times 6}\right)^{-1}\right]^{T}. \tag{9}$$

Equations (3)-(9) describe the relationships between the positions of the light spots on the PSDs and each 6DOF geometric errors, where N represents the number of experiments; X_{PSD1}, Y_{PSD1}, X_{PSD2}, Y_{PSD2}, X_{PSD3}, and Y_{PSD3} are the coordinate values for PSD_1, PSD_2, and PSD_3 in the X- and Y-directions, respectively; and $\boldsymbol{\beta}_{6\times 6}$ denotes the decoupling matrix of the proposed measurement system. From Eq. (9), the horizontal straightness error in the X-direction (δ_x), positioning error in the Y-direction (δ_y), vertical straightness error in the Z-direction (δ_z), pitch error about the X-axis (ε_x), roll error about the Y-axis (ε_y), and yaw error (ε_z) can be determined using the decoupling matrix $\boldsymbol{\beta}_{6\times 6}$. Because of the linear relationship between the PSD readings and 6DOF geometric errors, the function between them can be easily obtained through curve fitting (Fig. 8). After each function relating the PSDs and 6DOF geometric errors is obtained, the superposition principle can be used to obtain

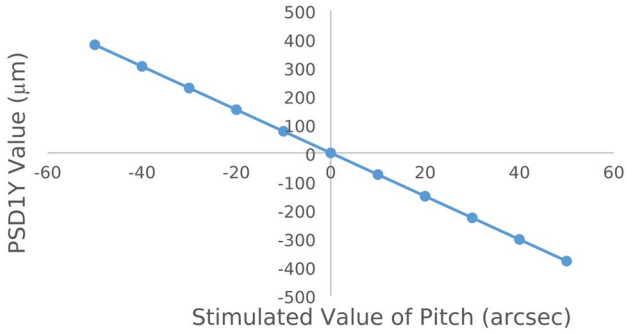

Fig. 8 Curve fitting of PSD_{1Y} and pitch error

a first degree equation (Eqs. (10)–(15)), and the coefficient of $\boldsymbol{\beta}_{6\times 6}$ can be determined:

$$\begin{aligned} \mathrm{X_{PSD1}} =& (\mathrm{A1}) * \varepsilon\mathrm{x} + (\mathrm{A2}) * \varepsilon\mathrm{y} + (\mathrm{A3}) * \varepsilon\mathrm{z} + (\mathrm{A4}) \\ & * \delta\mathrm{x} + (\mathrm{A5}) * \delta\mathrm{y} + (\mathrm{A6}) * \delta\mathrm{z}, \end{aligned} \tag{10}$$

$$\begin{aligned} \mathrm{Y_{PSD1}} =& (\mathrm{B1}) * \varepsilon\mathrm{x} + (\mathrm{B2}) * \varepsilon\mathrm{y} + (\mathrm{B3}) * \varepsilon\mathrm{z} + (\mathrm{B4}) \\ & * \delta\mathrm{x} + (\mathrm{B5}) * \delta\mathrm{y} + (\mathrm{B6}) * \delta\mathrm{z}, \end{aligned} \tag{11}$$

$$\begin{aligned} \mathrm{X_{PSD2}} =& (\mathrm{C1}) * \varepsilon\mathrm{x} + (\mathrm{C2}) * \varepsilon\mathrm{y} + (\mathrm{C3}) * \varepsilon\mathrm{z} + (\mathrm{C4}) \\ & * \delta\mathrm{x} + (\mathrm{C5}) * \delta\mathrm{y} + (\mathrm{C6}) * \delta\mathrm{z}, \end{aligned} \tag{12}$$

$$\begin{aligned} \mathrm{Y_{PSD2}} =& (\mathrm{D1}) * \varepsilon\mathrm{x} + (\mathrm{D2}) * \varepsilon\mathrm{y} + (\mathrm{D3}) * \varepsilon\mathrm{z} + (\mathrm{D4}) \\ & * \delta\mathrm{x} + (\mathrm{D5}) * \delta\mathrm{y} + (\mathrm{D6}) * \delta\mathrm{z}, \end{aligned} \tag{13}$$

$$\begin{aligned} \mathrm{X_{PSD3}} =& (\mathrm{E1}) * \varepsilon\mathrm{x} + (\mathrm{E2}) * \varepsilon\mathrm{y} + (\mathrm{E3}) * \varepsilon\mathrm{z} + (\mathrm{E4}) \\ & * \delta\mathrm{x} + (\mathrm{E5}) * \delta\mathrm{y} + (\mathrm{E6}) * \delta\mathrm{z}, \end{aligned} \tag{14}$$

Fig. 7 Schematic diagram of skew-ray tracing

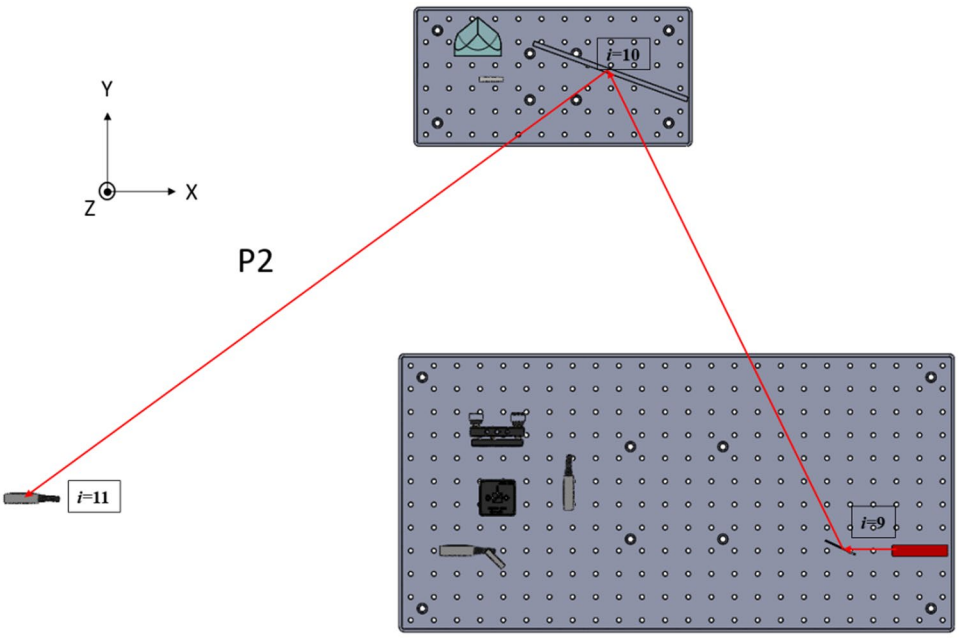

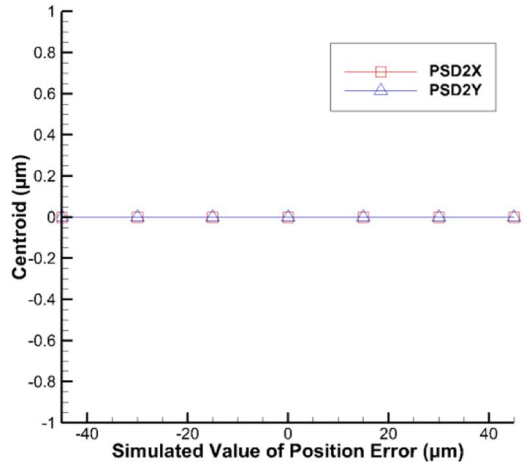
PSD2X
PSD2Y
Centroid (μm)
Simulated Value of Position Error (μm)

(a)

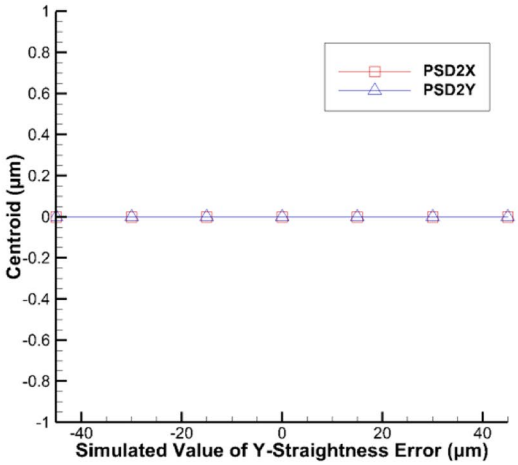
PSD2X
PSD2Y
Centroid (μm)
Simulated Value of Y-Straightness Error (μm)

(b)

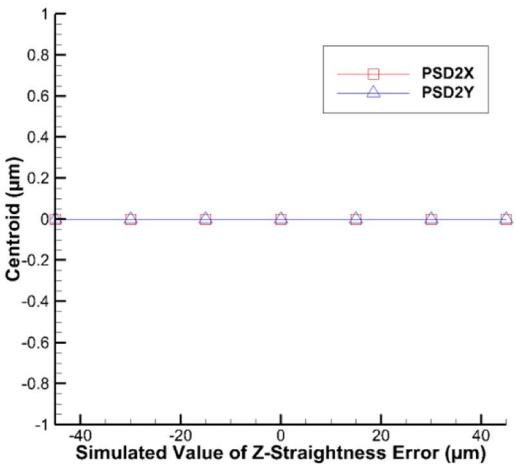
PSD2X
PSD2Y
Centroid (μm)
Simulated Value of Z-Straightness Error (μm)

(c)

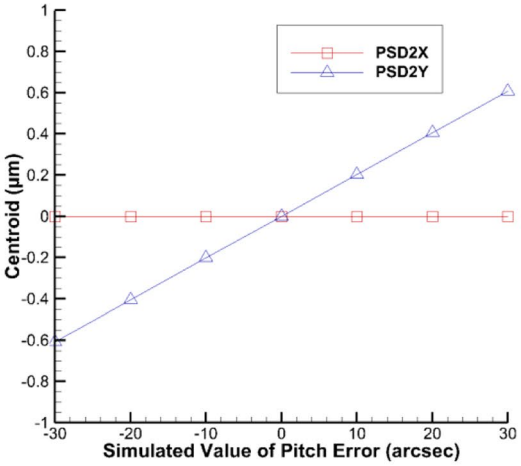
PSD2X
PSD2Y
Centroid (μm)
Simulated Value of Pitch Error (arcsec)

(d)

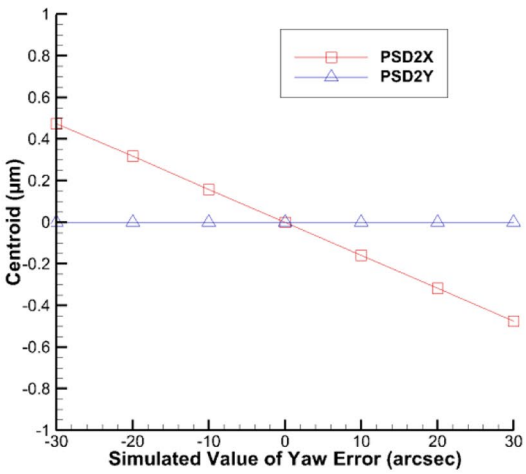
PSD2X
PSD2Y
Centroid (μm)
Simulated Value of Yaw Error (arcsec)

(e)

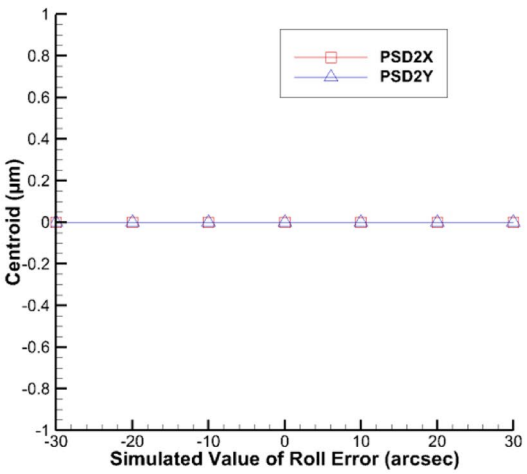
PSD2X
PSD2Y
Centroid (μm)
Simulated Value of Roll Error (arcsec)

(f)

◂**Fig. 9** Influence of (**a**) positioning errors, (**b**) horizontal straightness, (**c**) vertical straightness, (**d**) pitch, (**e**) yaw, and (**f**) roll in extra linear stage, respectively, on PSD2

$$Y_{PSD3} = (F1) * \varepsilon x + (F2) * \varepsilon y + (F3) * \varepsilon z + (F4) * \delta x + (F5) * \delta y + (F6) * \delta z. \quad (15)$$

5 Error analysis of additional linear stage

As mentioned previously, the 6DOF geometric errors of the additional linear stage may influence the readings of PSD2 (Fig. 9). The position, horizontal straightness, vertical straightness, and roll errors do not affect the PSD2 readings; although the pitch and yaw errors may affect the accuracy of the system, they are sufficiently small to be ignored because the proposed measurement approach involves subtracting the initial position of the additional stage from its end position, resulting in minimal geometric errors for a displacement d of 4 mm. Given that, their influence to the measurement accuracy of the proposed measurement system is ignored.

6 Compensating for systematic error

The proposed measurement system may incur additional uncertainties, such as installation and manufacturing errors. The optical simulation results may therefore differ from those of actual situations. A precise Newport XP50-MECA (six-axis Stewart platform, Fig. 10) was used to generate accurate 6DOF motion to simulate the 6DOF geometric errors of a linear stage. Although the Newport XP50-MECA includes 6DOF error in its movement, its specifications indicate that its bidirectional repeatability in the X-, Y-, and Z-directions of $\pm 0.60, \pm 0.60, \pm 0.30$ μm, respectively, and bidirectional repeatability (Θ) about the x-, y-, and z-axes of $\pm 0.30, \pm 0.30$, and ± 0.60 mdeg, respectively, which are considerably smaller than the geometric errors of a machine tool's linear stage [33]. Consequently, the Newport XP50-MECA is an ideal mobile platform. The ideal errors of the Stewart platform are then used to decouple the matrix $\boldsymbol{\beta}_{6\times6}$ using the least-squares method of $\text{Error}_{N\times6}$ and $\text{PSD}_{N\times6}$. We tested the accuracy of the decoupling matrix $\boldsymbol{\beta}_{6\times6}$ by decoupling the

Table 1 Coordinate transformation matrix parameters

I	$i=9$	$i=10$	$i=11$
Optical Element	BS	Mirror1	PSD2
N_i	Reflected	Reflected	Reflected
I_{ix}	cos(141°)	cos(-13°)	cos(180°)
I_{iy}	-sin(141°)	-sin(-13°)	-sin(180°)
I_{iz}	0	0	0
J_{ix}	sin(141°)	sin(-13°)	sin(180°)
J_{iy}	cos(141°)	cos(-13°)	cos(180°)
J_{iz}	0	0	0
K_{ix}	0	0	0
K_{iy}	0	0	0
K_{iz}	1	1	1
t_{ix}	$L9_x$	$L10_x$	$L11_x$
t_{iy}	$L9_y$	$L10_y$	$L11_y$
t_{iz}	$L9_z$	$L10_z$	$L11_z$

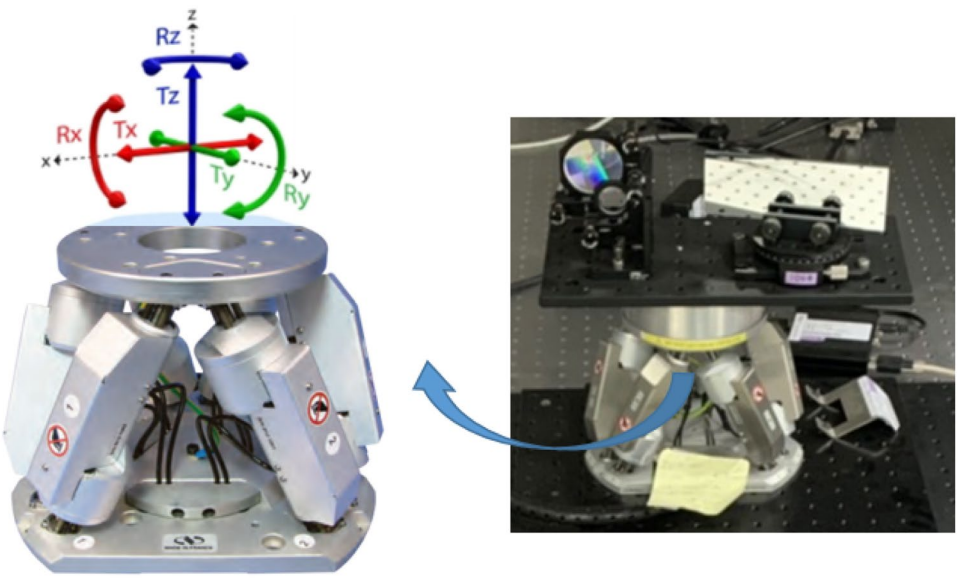

Fig. 10 6DOF motion of Newport HXP50-MECA

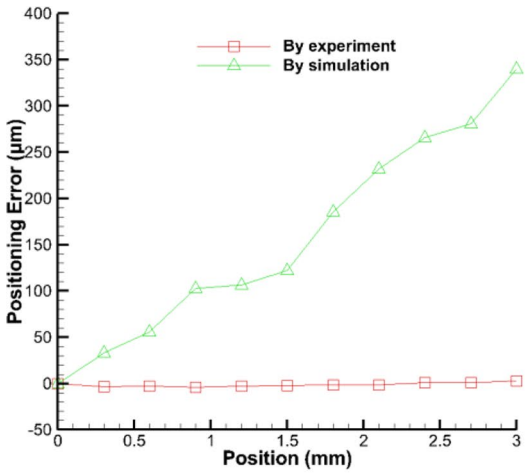
By experiment
By simulation
Positioning Error (μm)
Position (mm)

(a)

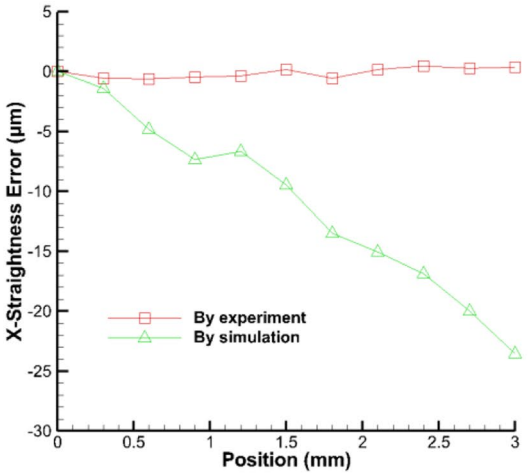
By experiment
By simulation
X-Straightness Error (μm)
Position (mm)

(b)

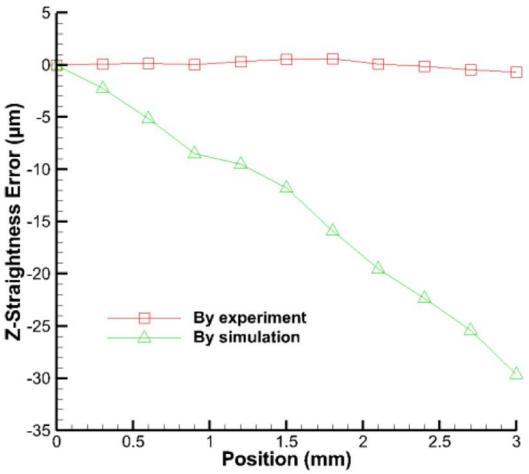
By experiment
By simulation
Z-Straightness Error (μm)
Position (mm)

(c)

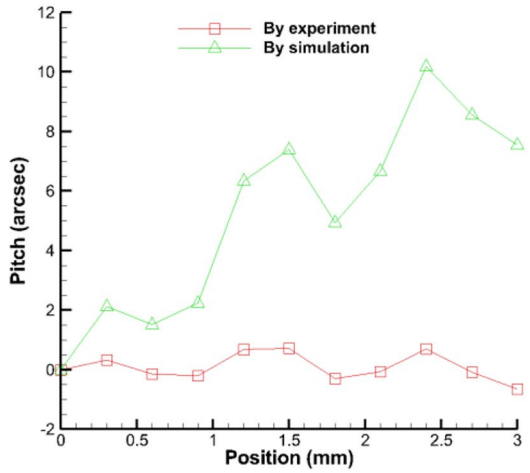
By experiment
By simulation
Pitch (arcsec)
Position (mm)

(d)

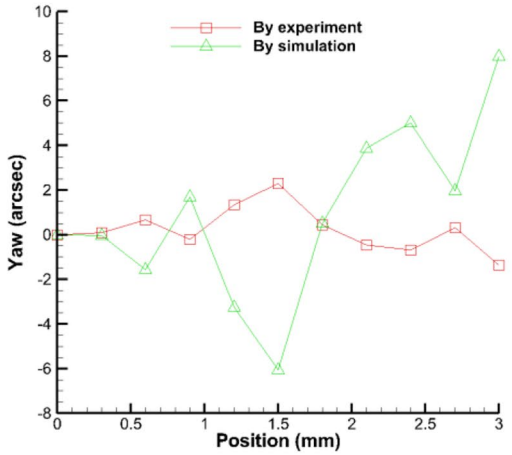
By experiment
By simulation
Yaw (arcsec)
Position (mm)

(e)

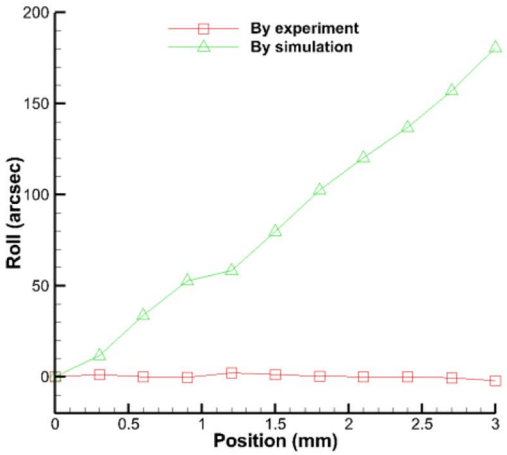
By experiment
By simulation
Roll (arcsec)
Position (mm)

(f)

◂**Fig. 11** The comparison of two decouple matrices, (**a**) positioning, (**b**) horizontal straightness, (**c**) vertical straightness, (**d**) pitch, (**e**) yaw, and (**f**) roll errors, respectively

6DOF geometric errors of the Stewart platform. Because the Stewart platform is a precise mobile platform, when it is moving, the measured 6DOF geometric errors are approximately zero. The simulated and the experimental decoupling matrices are compared in Fig. 11. The results indicate that the experimental decoupling matrix is more accurate than the simulated matrix because the 6DOF geometric errors of the Stewart platform are closer to zero.

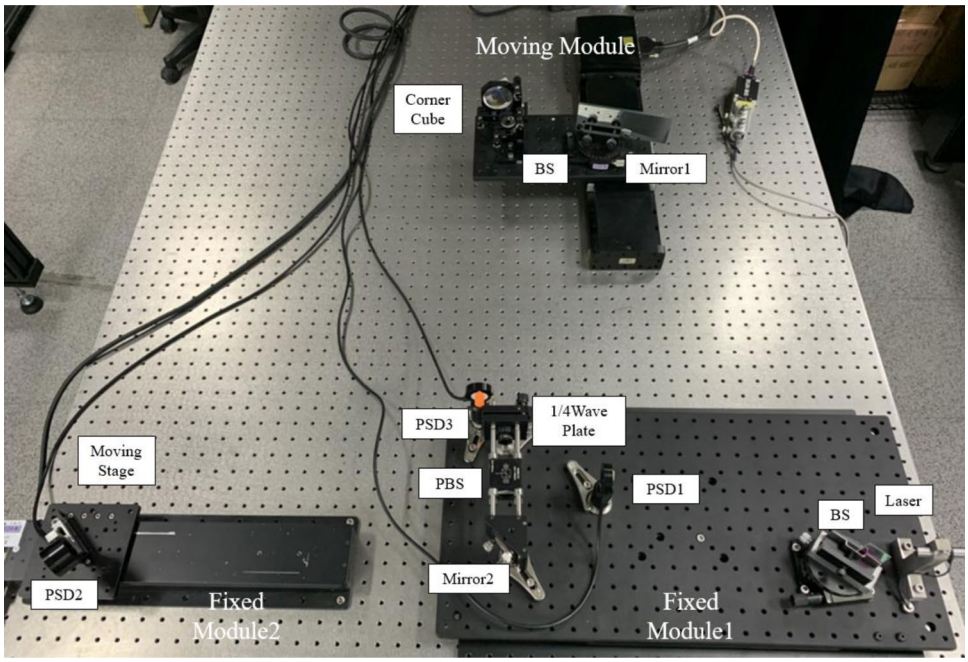

Fig. 12 Photograph of laboratory-built prototype

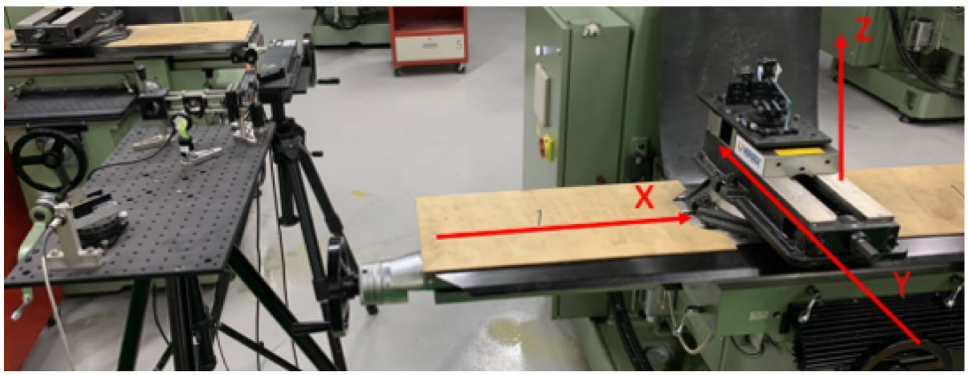

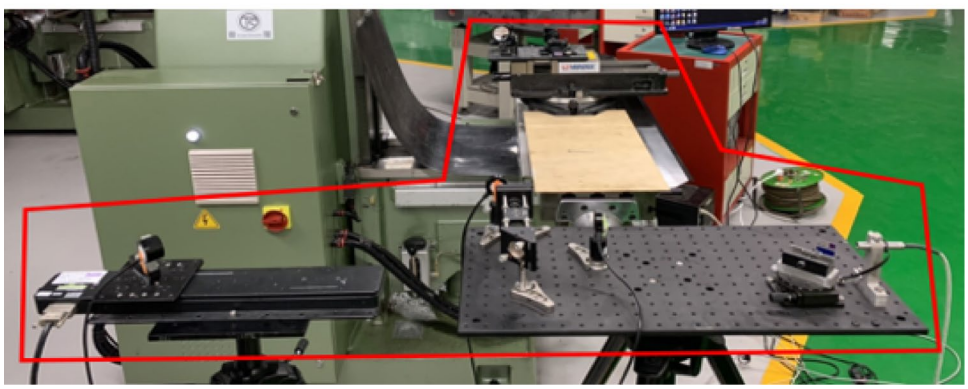

Fig. 13 Proposed prototype installed in milling machine

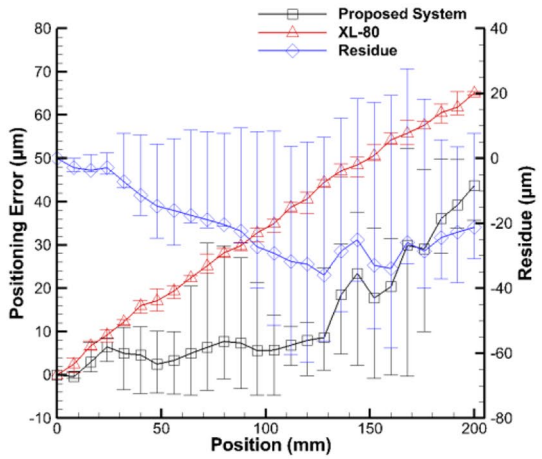
Proposed System
XL-80
Residue
Positioning Error (μm)
Residue (μm)
Position (mm)

(a)

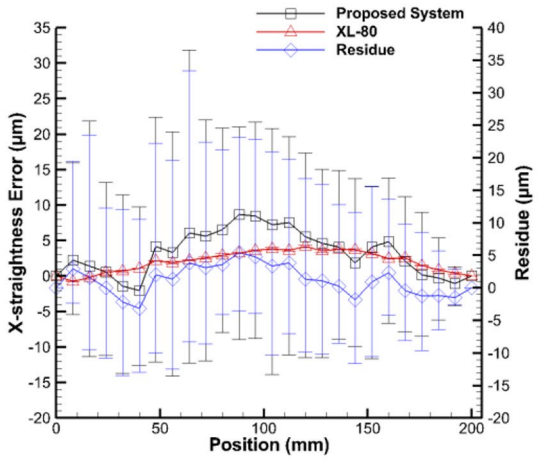
Proposed System
XL-80
Residue
X-straightness Error (μm)
Residue (μm)
Position (mm)

(b)

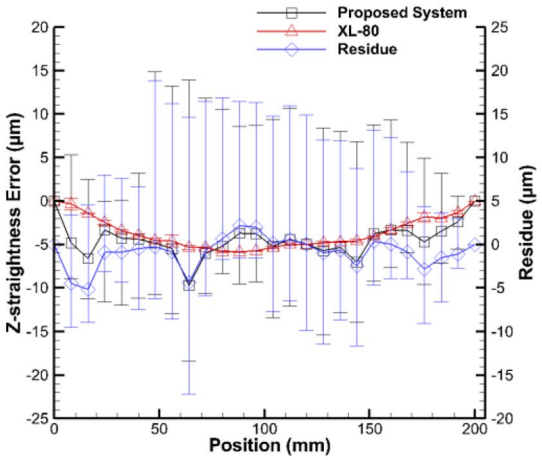
Proposed System
XL-80
Residue
Z-straightness Error (μm)
Residue (μm)
Position (mm)

(c)

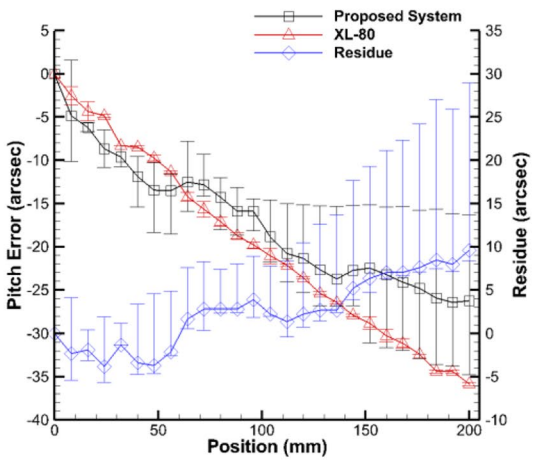
Proposed System
XL-80
Residue
Pitch Error (arcsec)
Residue (arcsec)
Position (mm)

(d)

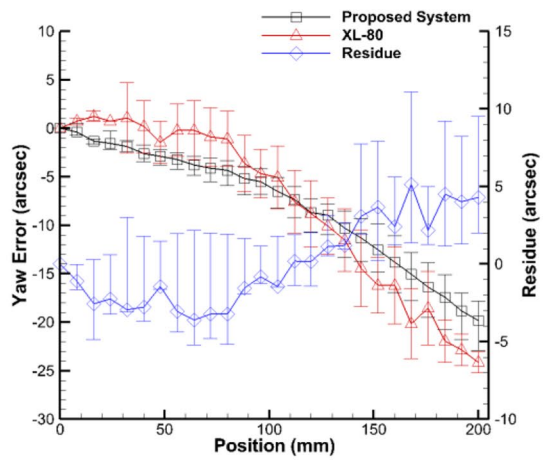
Proposed System
XL-80
Residue
Yaw Error (arcsec)
Residue (arcsec)
Position (mm)

(e)

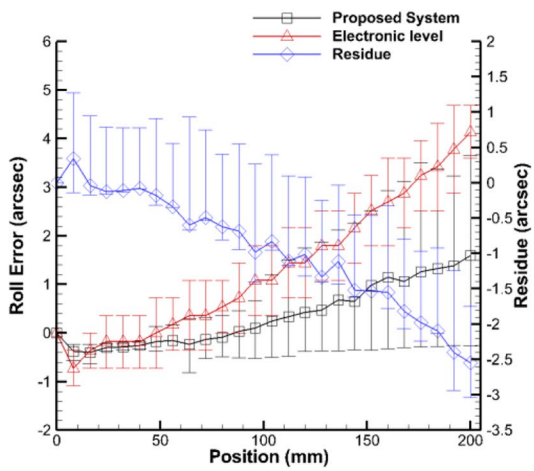
Proposed System
Electronic level
Residue
Roll Error (arcsec)
Residue (arcsec)
Position (mm)

(f)

◂**Fig. 14** Measurement results for variation of geometric error with position (**a**) positioning, (**b**) horizontal straightness, (**c**) vertical straightness, (**d**) pitch, (**e**) yaw, and (**f**) roll error, respectively

7 Experimental verification

The feasibility of the proposed measurement system was demonstrated through testing of a laboratory-built prototype (Fig. 12), which was used to simultaneously measure the 6DOF geometric errors of a milling machine's linear stage (LC-1 1/2, First, Taichung, Taiwan; Fig. 13). A Renishaw XL-80 interferometer and a DL-S3 electronic level (for measuring the roll error) were used to measure the 6DOF geometric errors of the linear stage and test the accuracy of the proposed measurement system.

Figure 14 presents a series of measurement results obtained by the proposed measurement system or Renishaw XL-80 interferometer and electronic level, showing five repeated measurements (200 mm) at each position. For the measured linear stage, the repeatability for the positioning, *X*-straightness, *Z*-straightness, pitch, yaw, and roll errors were 52.5 μm, 44 μm, 32.3 μm, 18.5 arcsec, 5.86 arcsec, and 3.91 arcsec, respectively.

The proposed measurement system has poorer accuracy than the commercial instruments, but their trends are similar because the measurement accuracy of the proposed measurement system is influenced not only by laser beam fluctuations but also by PSD sensitivity, misalignments, aberrations, and Abbe errors [14, 34]. For instance, laser beam instability and stray light in the environment could influence the measurement results during experiments. The timing fluctuations of the laser source introduce noise, further degrading the measurement accuracy. However, methods can be used to measure and compensate for such fluctuations in beam geometry [23], and a color filter can be used to control the light projecting onto the PSDs and thereby reduce the influence of stray light from the environment. Overcoming these limitations thus can improve the accuracy of the proposed measurement system in the future.

8 Conclusion

The proposed measurement system is designed for long-range measurement of the 6DOF geometric errors of a linear stage through geometrical optics; the system successfully overcomes the challenges of using geometrical optics for such measurement. The system is inexpensive and has a simple structure. In addition, a method of compensating for systematic errors is proposed. Compared with a Renishaw XL-80 interferometer, the proposed measurement system is less expensive and less time-consuming to use; moreover, it can measure 6DOF geometric errors simultaneously. The performance of the proposed measurement system was demonstrated with a laboratory-built prototype, and the repeatability for positioning, *X*-direction straightness, *Z*-direction straightness, pitch, yaw, and roll errors were 52.5 μm, 44 μm, 32.3 μm, 18.5 arcsec, 5.86 arcsec, and 3.91 arcsec, respectively.

Author contributions Wei-Che Tai was involved in writing—original draft preparation, conceptualization, methodology, software, validation. Chien-Sheng Liu helped in writing—reviewing and editing, supervision, project administration.

Funding The authors gratefully acknowledge the financial support provided to this study by the Ministry of Science and Technology of Taiwan under Grant Nos. MOST 106–2628-E-006–010-MY3 and 110–2221-E-006–126-MY3.

Availability of data and materials Not applicable.

Declarations

Ethical approval Not applicable.

Consent to participate Not applicable.

Consent to publish Not applicable.

Competing interests The authors have no financial or proprietary interests in any material discussed in this article.

References

1. Chen YT, More P, Liu CS, Cheng CC (2019) Identification and compensation of position-dependent geometric errors of rotary axes on five-axis machine tools by using a touch-trigger probe and three spheres. Int J Adv Manuf Technol 102:3077–3089
2. Chen YT, More P, Liu CS (2019) Identification and verification of location errors of rotary axes on five-axis machine tools by using a touch-trigger probe and a sphere. Int J Adv Manuf Technol 100:2653–2667
3. de Lacalle NL, Mentxaka AL (2009) Machine tools for high performance machining. Springer, London
4. Peng WC, Xia HJ, Wang SJ, Chen XD (2018) Measurement and identification of geometric errors of translational axis based on sensitivity analysis for ultra-precision machine tools. Int J Adv Manuf Technol 94(5–8):2905–2917
5. Fan KC, Chen MJ, Huang WM (1998) A six-degree-of-freedom measurement system for the motion accuracy of linear stages. Int J Mach Tools Manuf 38:155–164
6. Huang YB, Fan KC, Lou ZF, Sun W (2020) A novel modeling of volumetric errors of three-axis machine tools based on Abbe and Bryan principles. Int J Mach Tools Manuf 151:103527
7. Guo S, Jiang G, Mei X (2017) Investigation of sensitivity analysis and compensation parameter optimization of geometric error for five-axis machine tool. Int J Adv Manuf Technol 93:3229–3243
8. Li QZ, Wang W, Zhang J, Shen R, Li H, Jiang Z (2019) Measurement method for volumetric error of five-axis machine tool considering measurement point distribution and adaptive identification process. Int J Mach Tools Manuf 147:103465

9. Cheng Q, Zhao H, Zhao Y, Sun B, Gu P (2018) Machining accuracy reliability analysis of multi-axis machine tool based on Monte Carlo simulation. J Intell Manuf 29:191–209
10. Liu H, Xiang H, Chen J (2018) Measurement and compensation of machine tool geometry error based on Abbe principle. Int J Adv Manuf Technol 98:2769–2774
11. Gao W, Weng L, Zhang J (2020) An improved machine tool volumetric error compensation method based on linear and squareness error correction method. Int J Adv Manuf Technol 106:4731–4744
12. Aguado S, Samper D, Santolaria J, Aguilar JJ (2012) Identification strategy of error parameter in volumetric error compensation of machine tool based on laser tracker measurements. Int J Mach Tools Manuf 53:160–169
13. Gomez-Acedo E, Olarra A, Zubieta M et al (2015) Method for measuring thermal distortion in large machine tools by means of laser multilateration. Int J Adv Manuf Technol 80:523–534
14. Chen YT, Lin WC, Liu CS (2017) Design and experimental verification of novel six-degree-of freedom geometric error measurement system for linear stage. Opt Lasers Eng 92:94–104
15. Feng Q, Zhang B, Cui C, Kuang C, Zhai Y, You F (2013) Development of a simple system for simultaneously measuring 6DOF geometric motion errors of a linear guide. Opt Express 21:25805–25819
16. Wang W, Kweon SH, Hwang CS, Kang NC, Kim YS, Yang SH (2009) Development of an optical measuring system for integrated geometric errors of a three-axis miniaturized machine tool. Int J Adv Manuf Technol 43:701–709
17. Gao S, Zhang B, Feng Q, Cui C, Chen S, Zhao Y (2015) Errors crosstalk analysis and compensation in the simultaneous measuring system for five-degree-of-freedom geometric error. Appl Optics 54:458–466
18. Ramesh R, Mannan MA, Poo AN (2000) Error compensation in machine tools—a review: Part I: geometric, cutting-force induced and fixture-dependent errors. Int J Mach Tools Manuf 40:1235–1256
19. Huang P, Li Y, Wei H, Ren L, Zhao S (2013) Five-degrees-of-freedom measurement system based on a monolithic prism and phase-sensitive detection technique. Appl Opt 52:6607–6615
20. Zhang T, Feng Q, Cui C, Zhang B (2014) Research on error compensation method for dual-beam measurement of roll angle based on rhombic prism. Chin Opt Lett 12:071201
21. Furutani R (2017) Measurement of six-degree motion error of linear stage. IOP Conf Ser Mater Sci Eng 211:012001
22. Liu CS, Lai JJ, Luo YT (2019) Design of a measurement system for six-degree-of-freedom geometric errors of a linear guide of a machine tool. Sensors 19:5
23. Liu CS, Pu YF, Chen YT, Luo YT (2018) Design of a measurement system for simultaneously measuring six-degree-of-freedom geometric errors of a long linear stage. Sensors 18:3875
24. Chen JS, Kou TW, Chiou SH (1999) Geometric error calibration of multi-axis machines using an auto-alignment laser interferometer. Precis Eng 23:243–252
25. Gao S, Zhang B, Feng Q (2015) Errors crosstalk analysis and compensation in the simultaneous measuring system for five-degree-of-freedom geometric error. Appl Opt 54:458–466
26. Zhao Y, Zhang B, Feng Q (2017) Measurement system and model for simultaneously measuring 6DOF geometric errors. Opt Express 25:20993–21007
27. Zheng F, Feng Q, Zhang B, Li J, Zhao Y (2020) A high-precision laser method for directly and quickly measuring 21 geometric motion errors of three linear axes of computer numerical control machine tools. Int J Adv Manuf Technol 109:1285–1296
28. Huang Y, Fan KC, Sun W (2019) Embedded sensor system for five-degree-of-freedom error detection on machine tools. Mech Eng Sci 1(2):8–17
29. Liu CS, Zeng JY, Chen YT (2021) Development of positioning error measurement system based on geometric optics for long linear stage. Int J Adv Manuf Technol 115:2595–2606
30. Zheng F, Feng Q, Zhang B, Li J, Zhao Y (2020) Effect of detector installation error on the measurement accuracy of multi-degree-of-freedom geometric errors of a linear axis. Meas Sci Technol 31:094018
31. Cui FK, Song ZB, Wang XQ, Zhang FS, Li Y (2010) Study on Laser Triangulation Measurement Principle of Three Dimensional Surface Roughness. Adv Mater Res 136:91–94
32. Lin PD (2014) New computation methods for geometrical optics. Springer, Singapore
33. Newport, HXP50-MECA [Online]. Available: https://www.newport.com/p/HXP50-MECA
34. Rodríguez-Navarro D, Lázaro-Galilea JL, Bravo-Muñoz I, Gardel-Vicente A, Tsirigotis G (2016) Analysis and calibration of sources of electronic error in PSD sensor response. Sensors 16:619